Lambda hypernuclei and neutron star matter in a chiral SU(3) relativistic mean field model with a logarithmic potential

K. Tsubakihara,[1,*] H. Maekawa,[1] H. Matsumiya,[1] and A. Ohnishi[2]

[1] *Department of Physics, Faculty of Science, Hokkaido University, Sapporo 060-0810, Japan.*
[2] *Yukawa Institute for Theoretical Physics, Kyoto University, Kyoto 606-8502, Japan.*

(Dated: April 27, 2010)

We develop a chiral SU(3) symmetric relativistic mean field (RMF) model with a logarithmic potential of scalar condensates. Experimental and empirical data of symmetric nuclear matter saturation properties, bulk properties of normal nuclei, and separation energies of single- and double-Λ hypernuclei are well explained. The nuclear matter equation of state (EOS) is found to be softened by $\sigma\zeta$ mixing which comes from determinant interaction. The neutron star matter EOS is further softened by Λ hyperons.

I. INTRODUCTION

The equation of state (EOS) of the dense hadronic matter is one of the keys in nuclear physics as well as in physics of compact stars [1–14]. In dense matter, various forms of matter are expected to appear such as the hyperon admixture [4–10], meson condensation [11, 12], baryon rich quark gluon plasma [13], and color superconductor [14]. Among these exotic forms of matter, hyperons are expected to appear at relatively small densities, $\sim (2-3)\rho_0$. In addition to the variety of particle species, partial restoration of chiral symmetry is also expected in nuclear medium, and it would modify the properties of dense matter significantly. Therefore, it is desired to respect both hypernuclear physics information [15–19] and chiral symmetry [20–22] in constructing the dense matter EOS.

It is widely believed that hyperons should emerge such as in the neutron star core [4, 6–10], and/or during the black hole formation [23], as the baryon density increases in the hadronic matter. In neutron stars, hyperon admixtures soften the EOS and reduce the maximum mass of neutron stars. They also increase the proton fraction, which may promote faster cooling processes [24]. In black hole formation processes, hyperons are abundantly produced due to temperature or density effects, and shorten the duration time of neutrino emission [23]. Hyperon admixtures are governed by the hyperon potentials in nuclear matter, which may be determined from the hyperon separation energies from hypernuclei and hyperon production spectra. From this point of view, we need to adopt a theoretical framework which can explain both nuclear matter and finite nuclear properties.

A chiral symmetry is another important ingredient in dense matter. It is a fundamental symmetry of QCD with massless quarks, and its spontaneous symmetry breaking generates masses of constituent quarks and hadrons [20]. Hadron properties and EOS would be modified in nuclear matter due to the partial restoration of the chiral symmetry [21]. Thus it is preferable for hadronic many-body theories to possess the chiral symmetry, including its spontaneous breaking and partial restoration at finite densities.

We have recently developed a chiral SU(2) symmetric relativistic mean field (RMF) model, abbreviated as SCL2 RMF, with a logarithmic σ potential in the form of $-\log\sigma$ [25], which is derived from the strong coupling limit of lattice QCD (SCL-LQCD) [26, 27]. If we naïvely include the vector meson in the linear σ model (ϕ^4 theory), the chiral symmetry is found to be restored below the normal nuclear density (Lee-Wick vacuum, or chiral collapse) [28, 29]. To avoid this problem, there are several attempts some of which result in having instability at large σ values [30] or too stiff EOS [31]. In the SCL2 RMF, we do not have any instability in the σ potential, and the obtained nuclear matter EOS is found to be reasonably soft. In addition, the bulk properties of finite nuclei (binding energies and charge rms radii) are well described. Then it is desired to extend the SCL2 to the $\mathrm{SU}_f(3)$ version in order to describe hypernuclear systems. We expect that this extension enables us to get detailed information of various hypernuclei.

In this paper, we introduce a chiral SU(3) symmetric RMF model, abbreviated as SCL3 RMF in the later discussion, as an extension of SCL2 RMF. Some of the model parameters are constrained by chiral symmetry through the hadron masses and vacuum condensates, and some of them are determined by the nuclear matter and finite nuclear properties. We also determine remaining parameters, meson-Λ coupling constants, by adopting the $\mathrm{SU}_f(3)$ symmetric relation for vector couplings and fitting existing Λ hypernuclear data for scalar couplings. We show that we can reproduce the separation energies of single Λ hypernuclei (S_Λ) [18] and the $\Lambda\Lambda$ bond energy ($\Delta B_{\Lambda\Lambda}$) in ${}^{6}_{\Lambda\Lambda}$He [19] by choosing the coupling constants appropriately. The EOS of symmetric matter is found to be softened by the scalar meson with hidden strangeness, $\zeta = \bar{s}s$, which couples with σ through the determinant interaction representing the effects of $\mathrm{U}_A(1)$ anomaly [32, 33]. We also discuss the neutron star matter EOS and neutron star maximum mass in the present SCL3 RMF.

*tsubaki@nucl.sci.hokudai.ac.jp

It is generally preferable to derive the dense matter EOS from bare baryon-baryon interactions. Non-relativistic calculations based on the variational method [34, 35] and the g-matrix [36–39] have been carried out based on realistic bare baryon-baryon interactions. These non-relativistic microscopic calculations only with two body forces do not reproduce the nuclear matter saturation point, and three-body forces are found to be essential to explain the saturation property of symmetric nuclear matter [34–39]. In Ref. [38, 39], the modern microscopic *NN*, *YN*, and *YY* interactions were examined with three-body forces in the framework of Brückner Hartree-Fock theory. The calculated results of the maximum neutron star mass suggest the importance of the hyperon admixture and the three-body force in neutron star core. In the relativistic Brückner Hartree-Fock (RBHF) theory [40], empirical nuclear matter saturation is explained quantitatively. It should be noted that a part of the three-body force effects are taken into account in RBHF via Z-type diagrams which come from relativistic treatments, but RBHF results in Ref. [40] do not include the bare three-body forces such as those via baryon resonances. The EOS in RBHF is approximately reproduced in RMF with non-linear ω interaction, which is introduced to simulate the high density behavior of the vector potential [41]. In this work, we follow the latter stand point: We start from the Lagrangian with several model parameters and determine these parameters by fitting existing data. As a result, the scalar and vector potentials in a symmetric nuclear matter are found to be consistent with the RBHF results, then we expect that the results with hyperons would be also meaningful.

This paper is organized as follows. In Sec. II, we introduce a chiral SU(3) potential derived from SCL-LQCD in RMF as an extension from the chiral SU(2) potential. In Sec. III, we investigate the properties of symmetric nuclear matter, normal nuclei, and Λ hypernuclei, and fix the parameters in RMF model so as to reproduce empirical and experimental data. Then, we can anticipate neutron star matter EOS with an RMF model which can explain experimental data. Finally, we summarize our results and give an outlook. in Sec. IV.

II. CHIRAL SU(3) RMF MODEL

An energy density as a function of the chiral condensate, abbreviated as a *chiral potential* here, describes the spontaneous chiral symmetry breaking and its partial restoration through the chiral condensates, and these chiral condensates determine hadron masses. In Ref. [25], Tsubakihara and Ohnishi proposed to apply the logarithmic chiral SU(2) potential derived from the strong coupling limit of lattice QCD (SCL-LQCD) and developed the SCL2 RMF model. In Subsec. II A, we briefly summarize how to derive the chiral potential in SCL-LQCD [25, 26]. Extension to a chiral SU(3) potential is described in Subsec. II B, and a chiral SU(3) symmetric RMF is introduced in Subsec. II C.

A. Chiral SU(2) Potential from SCL-LQCD (SCL2)

The lattice QCD action consists of the pure Yang-Mills part and the fermionic part. The pure Yang-Mills part is proportional to $1/g^2$, where g is the bare QCD coupling. In SCL-LQCD ($g \to \infty$), we can ignore the pure Yang-Mills action terms, and only those terms including fermions S_F are kept in the action [26]. The fermionic action with staggered fermions in the chiral limit is written in the lattice unit as,

$$S_F[\chi,\bar{\chi},U] = \frac{1}{2}\sum_{x,\mu}\eta_\mu(x)\left[\bar{\chi}(x)U_\mu(x)\chi(x+\hat{\mu}) - \bar{\chi}(x+\hat{\mu})U_\mu^\dagger(x)\chi(x)\right] , \tag{1}$$

where $\eta_\mu(x) = (-1)^{x_0+x_1+\cdots+x_{\mu-1}}$ represents the staggered factor. After integrating out link variables U_μ in the leading order of $1/d$ expansion [26], we obtain the following partition function $\mathcal{Z}$,

$$\begin{aligned}\mathcal{Z} &= \int \mathcal{D}[\chi,\bar{\chi},U]\exp\left(-S_F[\chi,\bar{\chi},U]\right)\\ &\simeq \int \mathcal{D}[\chi,\bar{\chi}]\exp\left[\frac{1}{2}\sum_{x,y,\alpha,\beta}\mathcal{M}_{\alpha\beta}(x)V_M(x,y)\mathcal{M}(y)_{\beta\alpha}\right]\\ &= \int \mathcal{D}[\chi,\bar{\chi},\sigma]\exp\left(-S_\sigma[\chi,\bar{\chi},\sigma]\right) , \end{aligned}\tag{2}$$

$$S_\sigma = \frac{1}{2}\sum_{x,y,\alpha,\beta}\sigma(x)_{\alpha\beta}V_M(x,y)\sigma(y)_{\beta\alpha} + \sum_{x,y,\alpha,\beta}\sigma(y)_{\alpha\beta}V_M(y,x)\mathcal{M}(x)_{\beta\alpha} . \tag{3}$$

The mesonic composites are defined as $\mathcal{M}_{\alpha\beta}(x) = \bar{\chi}^a_\beta(x)\chi^a_\alpha(x)$, and the auxiliary fields $\sigma_{\alpha\beta}$ are related to the expectation values of the mesonic composites, $\langle\sigma_{\alpha\beta}(x)\rangle = -\langle\mathcal{M}_{\alpha\beta}(y)\rangle$. In these equations, the superscript a denotes color and the subscripts α and β show the flavors of the quark fields. The lattice mesonic inverse propagator $V_M(x,y)$ is given as $V_M(x,y) = \sum_\mu\left(\delta_{y,x+\hat{\mu}} + \delta_{y,x-\hat{\mu}}\right)/4N_c$. From the first to the second line in Eq. (2), the one-link integral formula, $\int dU U_{ab}U^\dagger_{cd} = \delta_{ad}\delta_{bc}/N_c$ has been used.

Here, we substitute the auxiliary fields with the static and uniform scalar $\Sigma_{\alpha\beta}$ and pseudoscalar $\mathbf{\Pi}_{\alpha\beta}$ matrices as the mean field ansatz,

$$\sigma_{\alpha\beta}(x) = \Sigma_{\alpha\beta} + i\epsilon(x)\Pi_{\alpha\beta} , \tag{4}$$

where $\varepsilon(x) = (-1)^{x_0+x_1+x_2+x_3}$. Since fermions are decoupled in each space-time point, the grassmann integral can be easily evaluated and the effective free energy is

obtained up to a constant as,

$$V_\chi(\sigma,\boldsymbol{\pi}) = \frac{1}{2}\langle \mathrm{tr}\,[\sigma V_M \sigma]\rangle - N_c\langle \log\det(V_M\sigma)\rangle$$
$$= \frac{b_\sigma}{2}\mathrm{tr}\left[M^\dagger M\right] - \frac{a_\sigma}{2}\log\det\left[M^\dagger M\right] \ , \quad (5)$$
$$b_\sigma = \frac{d}{2N_c} \ , \quad a_\sigma = N_c \ , \quad (6)$$

where $\langle\cdots\rangle$ denotes the space-time average, $d=4$ is the space-time dimension, and M represents the meson matrix, $M=\Sigma_{\alpha\beta}+i\Pi_{\alpha\beta}$, in which the $\varepsilon(x)$ factor is replaced with unity in $\sigma_{\alpha\beta}$.

While the coefficients b_σ and a_σ are fixed in the lattice unit in Eq. (5), they depend on the lattice spacing and the scaling factor connecting the meson field and the quark condensate, which should be chosen for σ and $\boldsymbol{\pi}$ to be in the canonical form. Furthermore, n_f species of staggered fermions corresponds to $N_f = 4n_f$ flavors, and the coefficient modification may not be trivial when we take $N_f=2$ for SU(2) or $N_f = 2+1$ for SU(3). Thus we stipulate them as parameters to obtain physical meson masses.

In SU(2), meson matrix is given as $M=(\sigma+i\boldsymbol{\tau}\cdot\boldsymbol{\pi})/\sqrt{2}$. Requiring that the chiral potential has a minimum at $\sigma=f_\pi$ and fitting the pion mass m_π, one parameter m_σ is left as a free parameter. Then, the chiral potential is given as,

$$V_\chi = -\frac{a_\sigma}{2}\log\left(\det MM^\dagger\right) + \frac{b_\sigma}{2}\mathrm{tr}(MM^\dagger) - c_\sigma\sigma$$
$$= -a_\sigma\log(\sigma^2+\boldsymbol{\pi}^2) + \frac{b_\sigma}{2}(\sigma^2+\boldsymbol{\pi}^2) - c_\sigma\sigma$$
$$\simeq -2a_\sigma f_{\rm SCL}(\frac{\varphi_\sigma}{f_\pi}) + \frac{1}{2}m_\sigma^2\varphi_\sigma^2 + \frac{1}{2}m_\pi^2\boldsymbol{\pi}^2 \ , \quad (7)$$
$$f_{\rm SCL}(x) = \log(1-x) + x + \frac{x^2}{2} \ , \quad (8)$$

where $\varphi_\sigma = f_\pi - \sigma$, and the explicit chiral symmetry breaking term $-c_\sigma\sigma$ is introduced. We have omitted pion self-energy terms and constants in the third line in Eq. (7). Parameters a_σ, b_σ, c_σ are given as,

$$a_\sigma = \frac{f_\pi^2}{4}(m_\sigma^2 - m_\pi^2) \ , \ b_\sigma = \frac{1}{2}(m_\sigma^2+m_\pi^2) \ , \ c_\sigma = f_\pi m_\pi^2 \ , \quad (9)$$

With the above logarithmic σ potential, full chiral symmetry restoration is suppressed because of the repulsive contribution of V_χ at small σ. The present treatment of SCL-LQCD is referred to as the zero temperature treatment, where V_χ diverges at $\sigma\to 0$. In the finite temperature treatment of SCL-LQCD [27], the divergent behavior of V_χ disappears, while V_χ has a finite negative derivative at $\sigma\to 0$. This finite negative derivative is enough to suppress full chiral restoration at finite density, since the nucleon Fermi integral contribution behaves as $\rho_B\sigma^2$ and we always have a minimum at a finite σ value. Therefore, we suppose that the present chiral potential V_σ would be a good starting point to investigate cold nuclear matter and nuclei.

B. Chiral SU(3) potential from SCL-LQCD (SCL3)

In order to apply the logarithmic chiral potential to hypernuclear systems, it is necessary to include mesons with hidden strangeness ($\bar{s}s$) such as ζ and ϕ in addition to mesons made of u and d quarks (σ, ω and ρ). Here, we replace the meson matrix M with that of SU(3),

$$M = \begin{pmatrix} M_{11} & a_0^+ + i\pi^+ & \kappa^0 + iK^+ \\ a_0^- + i\pi^- & M_{22} & \kappa^0 + iK^0 \\ \kappa^- + iK^- & \bar{\kappa}^0 + i\bar{K}^0 & \zeta + i\eta_s \end{pmatrix} \ , \quad (10)$$
$$M_{11} \equiv \frac{1}{\sqrt{2}}\left[(\sigma+i\eta) + \left(a_0^0 + i\pi^0\right)\right] \ , \quad (11)$$
$$M_{22} \equiv \frac{1}{\sqrt{2}}\left[(\sigma+i\eta) - \left(a_0^0 + i\pi^0\right)\right] \ . \quad (12)$$

In a similar way to the previous subsection, the chiral SU(3) potential in SCL-LQCD may be given as,

$$V_\chi = -\frac{a'}{2}\log\left(\det M'M'^\dagger\right) + \frac{b'}{2}\mathrm{tr}\left(MM^\dagger\right)$$
$$- c_\sigma\sigma - c_\zeta\zeta + V_{\rm KMT} \ , \quad (13)$$

where the explicit chiral symmetry breaking effects are included as $c_\sigma\sigma$ and $c_\zeta\zeta$ terms. Since the strange quark mass is not small compared with f_π and f_ζ, we have taken account of its effects also in the shift of the meson matrix, $M' = M + \mathrm{diag}(0,0,\delta_s)$. This shifted meson matrix plays the role of the constituent quark mass in Eq. (3) and appears in the logarithmic term of the chiral potential.

The Kobayashi-Maskawa-'t Hooft interaction term [32, 33] is represented in a form of the determinant of meson matrix,

$$V_{\rm KMT} = -d'\left(\det M + \det M^\dagger\right) \ . \quad (14)$$

This KMT interaction represents the $\mathrm{U}_A(1)$ anomaly effects. Without $V_{\rm KMT}$, the above chiral potential is invariant under $\mathrm{U}_L(3)\times\mathrm{U}_R(3)$ transformation in the chiral limit, $\delta_s = c_\sigma = c_\zeta = 0$. In the real world, $\mathrm{U}_A(1)$ symmetry is broken by the anomaly. Kobayashi and Maskawa [32] proposed the above determinant interaction term, and this term is derived as the instanton induced quark interaction vertex by 't Hooft [33].

Now we shall decompose the chiral potential V_χ in

Eq. (13) into meson mass terms and interaction terms.

$$V_\chi = -a' \log(\sigma^2\zeta) + \frac{b'}{2}(\sigma^2+\zeta^2) - d'\sigma^2\zeta - c_\sigma\sigma - c_\zeta\zeta + \frac{1}{2}\sum_\alpha m_\alpha^2\phi_\alpha^2 + \delta V$$
$$= \frac{1}{2}m_\sigma^2\varphi_\sigma^2 + \frac{1}{2}m_\zeta^2\varphi_\zeta^2 + V_{\sigma\zeta}(\varphi_\sigma,\varphi_\zeta) + \frac{1}{2}\sum_\alpha m_\alpha^2\phi_\alpha^2 + \delta V(\varphi_\sigma,\varphi_\zeta,\{\phi_\alpha\}) + \text{const.}\ , \quad (15)$$

$$V_{\sigma\zeta} = -a'\left[2f_{\rm SCL}\left(\frac{\varphi_\sigma}{f_\pi}\right) + f_{\rm SCL}\left(\frac{\varphi_\zeta}{f'_\zeta}\right)\right] + \xi_{\sigma\zeta}\varphi_\sigma\varphi_\zeta\ , \quad (16)$$

where $\varphi_\sigma = f_\pi - \sigma$ and $\varphi_\zeta = f_\zeta - \zeta$ show the deviation of σ and ζ from their vacuum expectation values, respectively, and $V_{\sigma\zeta}$ denotes the interaction energy density. In the logarithmic potential, shifted vacuum expectation value of ζ reads $f'_\zeta = f_\zeta + \delta_s$. The other meson fields than σ and ζ are shown by ϕ_α, and m_α and δV represent their masses and interaction terms. We have ignored the third order term $(\varphi_\sigma)^2\varphi_\zeta$ coming from the determinant interaction. This term does not change the chiral potential significantly around the vacuum, but it makes the system unstable at large values of σ and ζ. This is because we do not have polynomial terms such as σ^4 and ζ^4, which stabilizes the chiral potential in the ϕ^4 theory. Compared with the case of SU(2), where all of $\mathrm{tr}(MM^\dagger)$, $\det M$ and $\det M^\dagger$ are proportional to the same combination, $\sigma^2+\boldsymbol{\pi}^2$, we have several different terms from $\log(\det M'M'^\dagger)$, $\mathrm{tr}(MM^\dagger)$ and $\det M + \det M^\dagger$ in SU(3).

In Eq. (15), the $\sigma\zeta$ mixing appears in the quadratic form of the meson fields, thus we have to diagonalize the mass matrix to obtain observed σ and ζ meson masses as

$$\frac{1}{2}\begin{pmatrix}\varphi_\sigma & \varphi_\zeta\end{pmatrix}\begin{pmatrix}m_\sigma^2 & \xi_{\sigma\zeta}\\ \xi_{\sigma\zeta} & m_\zeta^2\end{pmatrix}\begin{pmatrix}\varphi_\sigma\\ \varphi_\zeta\end{pmatrix} = \frac{1}{2}\begin{pmatrix}\varphi'_\sigma & \varphi'_\zeta\end{pmatrix}\begin{pmatrix}M_\sigma^2 & 0\\ 0 & M_\zeta^2\end{pmatrix}\begin{pmatrix}\varphi'_\sigma\\ \varphi'_\zeta\end{pmatrix}\ . \quad (17)$$

Five out of six (a', b', c_σ, c_ζ, d' and δ_s) parameters in this chiral potential are fixed by fitting observed meson masses of m_π, m_K and M_ζ, and vacuum expectation values of σ and ζ (f_π and f_ζ). Relevant meson masses are related to the parameters (a', b', d', δ_s) as,

$$m_\pi^2 = b' - \frac{2a'}{f_\pi^2} - 2d'f_\zeta\ , \quad (18)$$
$$m_\sigma^2 = b' + \frac{2a'}{f_\pi^2} - 2d'f_\zeta\ , \quad (19)$$
$$m_K^2 = b' - \frac{\sqrt{2}a'}{f_\pi f'_\zeta} - \sqrt{2}d'f_\pi\ , \quad (20)$$
$$m_\zeta^2 = b' + \frac{a'}{f'^2_\zeta}\ , \quad (21)$$
$$\xi_{\sigma\zeta} = -2d'f_\pi\ . \quad (22)$$

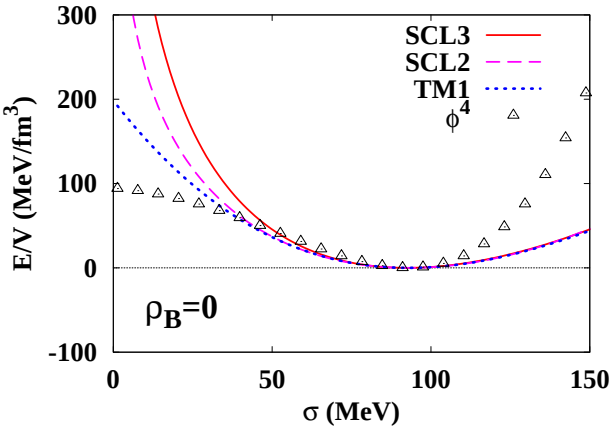

FIG. 1: (Color online) Energy density in vacuum as a function of σ in the SCL3 model (solid curve) is compared with those in the linear σ (ϕ^4, open-triangles), SCL2 (dashed curve), and TM1 (dotted curve) models.

We regard m_σ as a model parameter, and give a' and $b' - 2d'f_\zeta$ as in the case of the SCL2 model,

$$a' = \frac{f_\pi^2}{4}\left(m_\sigma^2 - m_\pi^2\right) = a_\sigma\ , \quad (23)$$
$$b' - 2d'f_\zeta = \frac{1}{2}\left(m_\sigma^2 + m_\pi^2\right) = b_\sigma\ . \quad (24)$$

We assign the observed ζ as $f_0(980)$, and the parameters b', d' and δ_s are determined to reproduce $m_\pi = 138$ MeV, $m_K = 496$ MeV and $M_\zeta = 980$ MeV.

Coefficients of the linear terms in σ and ζ are determined to reproduce the vacuum expectation values,

$$c_\sigma = f_\pi\left\{b' - \frac{2a'}{f_\pi^2} - 2d'f_\zeta\right\} = f_\pi m_\pi^2\ , \quad (25)$$
$$c_\zeta = b'f_\zeta - \frac{a'}{f'_\zeta} - f_\pi^2 d'\ . \quad (26)$$

Once we fix the parameters in the chiral SU(3) potential, masses of other scalar and pseudoscalar mesons are determined as shown in Appendix A. Calculated masses of these mesons are tabulated in Table I. They are in reasonable agreement with experimental values except for κ.

In Fig. 1, we show the energy density as a function of σ. We compare the SCL3 results with those in SCL2 [25], TM1 [41] and the linear σ (ϕ^4) models. We adopt the parameter $m_\sigma = 690$ MeV, which reproduces the bulk properties of normal nuclei as explained later, and optimal φ_ζ value is chosen for each σ. When we only consider the quadratic term in φ_σ, the energy density behaves as $m_\sigma^2\varphi_\sigma^2/2$. Thus the energy density in SCL3 can be twice larger than the results in SCL2 and TM1, in which m_σ is around 500 MeV, while the calculated results shows similar values around $\sigma = f_\pi$. This is because the optimal ζ value is chosen and reduces the energy density in SCL3. In Fig. 2, we show the energy surface as a function of φ_σ and φ_ζ. The optimal value of φ_ζ is modified

TABLE I: Parameters and masses of a_0, κ, η and η' mesons as functions of m_σ. Parameters are determined by fitting π, K and ζ masses ($m_\pi = 138$ MeV, $m_K = 496$ MeV, $M_\zeta = 980$ MeV), and vacuum condensate of σ and ζ ($f_\pi = 92.4$ MeV, $f_\zeta = 94.5$ MeV).

m_σ (MeV)	m_ζ (MeV)	a'/f_π^4	b'/f_π^2	d'/f_π	δ_s/f_π	m_{a_0} (MeV)	m_κ (MeV)	M_η (MeV)	$M_{\eta'}$ (MeV)	M_σ (MeV)
630	816.7	11.06	73.07	23.81	0.4568	1108.4	1000.8	536.0	1069.7	321.7
640	818.3	11.44	73.05	23.44	0.4364	1108.3	1000.7	535.7	1062.4	344.6
650	819.8	11.81	73.03	23.06	0.4175	1108.1	1000.5	535.4	1054.9	366.4
660	821.4	12.20	73.01	22.67	0.4001	1108.0	1000.3	535.0	1047.2	387.2
670	823.0	12.59	72.98	22.28	0.3840	1107.8	1000.1	534.6	1039.4	407.3
680	824.7	12.98	72.95	21.88	0.3690	1107.5	999.8	534.1	1031.3	426.7
690	826.3	13.38	72.92	21.47	0.3550	1107.3	999.6	533.6	1023.1	445.5
700	828.0	13.79	72.89	21.06	0.3421	1107.0	999.3	533.1	1014.6	463.8
710	829.6	14.20	72.85	20.64	0.3300	1106.8	999.0	532.5	1006.0	481.6
720	831.3	14.62	72.81	20.21	0.3187	1106.4	998.6	531.8	997.1	499.0
730	832.9	15.05	72.77	19.77	0.3081	1106.1	998.2	531.1	988.0	516.0
Exp.						980±20	672±40	547.85	957.78	400-1200

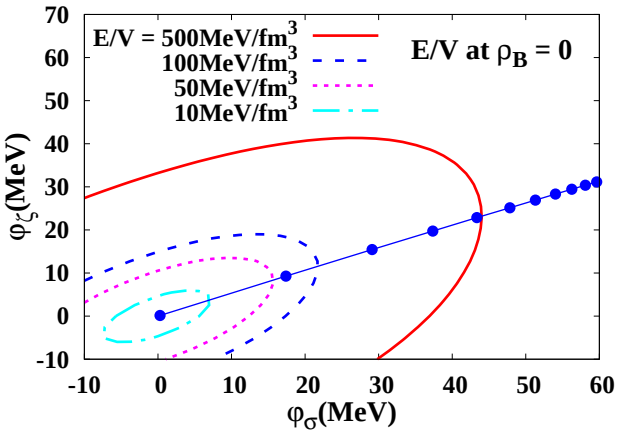

FIG. 2: (Color online) Energy surface of chiral effective potential $V_{\sigma\zeta}$ at $\rho_B = 0$ in SCL3. Points show chiral condensates (φ_σ and φ_ζ) at finite densities, $\rho_B/\rho_0 = 0, 0.5, \cdots 5$.

from zero to a finite value by the $\sigma\zeta$ coupling from the KMT interaction, and the energy density is reduced by this mixing.

C. SCL3 RMF model

We incorporate the chiral SU(3) potential $V_{\sigma\zeta}$ discussed in the previous subsections into the SU(3) RMF model. We consider the following SU(3) RMF Lagrangian, which describes baryons which couple with σ and $\zeta(=\bar{s}s)$ scalar mesons, and ω, ρ^0 (denoted by R), and ϕ vector mesons,

$$\begin{aligned}\mathcal{L} =& \sum_i \bar{\psi}_i \left[i\partial\!\!\!/ - M_i^* - \gamma_\mu U_i^\mu \right] \psi_i \\ &+ \frac{1}{2}\partial_\mu\varphi_\sigma\partial^\mu\varphi_\sigma - \frac{1}{2}m_\sigma^2\varphi_\sigma^2 + \frac{1}{2}\partial_\mu\varphi_\zeta\partial^\mu\varphi_\zeta - \frac{1}{2}m_\zeta^2\varphi_\zeta^2 \\ &- \frac{1}{4}\omega_{\mu\nu}\omega^{\mu\nu} + \frac{m_\omega^2}{2}\omega_\mu\omega^\mu - \frac{1}{4}R_{\mu\nu}R^{\mu\nu} + \frac{m_\rho^2}{2}R_\mu R^\mu \\ &- \frac{1}{4}\phi_{\mu\nu}\phi^{\mu\nu} + \frac{m_\phi^2}{2}\phi_\mu\phi^\mu - \frac{1}{4}F_{\mu\nu}F^{\mu\nu} \\ &+ \frac{c_\omega}{4}\left(\omega_\nu\omega^\nu\right)^2 - V_{\sigma\zeta}\left(\varphi_\sigma, \varphi_\zeta\right) \ , \end{aligned} \tag{27}$$

$$M_i^* = M_i - g_{\sigma i}\varphi_\sigma - g_{\zeta i}\varphi_\zeta \ , \tag{28}$$

$$U_i^\mu = g_{\omega i}\,\omega^\mu + g_{\rho i}\,R^\mu + \frac{1+\tau_3}{2}eA^\mu \ , \tag{29}$$

where $V^{\mu\nu}(V = \omega, R, \phi)$ shows the field tensor of the vector meson V. The ω^4 term in Eq. (27) is introduced to simulate the behavior of the vector potential at high densities in the RBHF theory [40, 41]. The term $V_{\sigma\zeta}(\varphi_\sigma, \varphi_\zeta)$ is the scalar self-interaction, and we adopt the chiral SU(3) potential $V_{\sigma\zeta}$ in Eq. (15).

In this Lagrangian, we have several model parameters to be fixed; m_σ in $V_{\sigma\zeta}$, c_ω for the ω self-interaction, and the meson-baryon coupling constants g_{mB}. We assume that (1) nucleon mass is fully generated by the chiral condensate, $M_N = g_{\sigma N} f_\pi$, (2) the vector couplings obey the $\mathrm{SU}_f(3)$ relation [15, 42], and (3) nucleon does not couple with hidden strangeness mesons (ζ and ϕ) [43, 44]. Suppressed $N\phi$ coupling is understood in the Okubo-Zweig-Iizuka (OZI) rule [43], while the scalar meson-nucleon coupling $g_{\zeta N}$ may violate the OZI rule [44]. Thus the assumption of $g_{\zeta N} = 0$ may be regarded as an working hypothesis.

TABLE II: Parameter set determined from saturation point of symmetric nuclear matter, binding energies and charge rms radii of normal nuclei, s_Λ of single Λ hypernuclei and $\Delta B_{\Lambda\Lambda}$ in ${}^{6}_{\Lambda\Lambda}$He. Input constants adopted in this paper are also shown. We adopt the saturation point, $(\rho_0, E_0/A) = (0.150\ \mathrm{fm}^{-3}, -16.3\ \mathrm{MeV})$.

m_σ (MeV)	δ_s (MeV)	$g_{\omega N}$	c_ω	$g_{\rho N}$	$g_{\sigma\Lambda}$	$g_{\zeta\Lambda}$
690	32.81	11.95	294.9	4.54	3.40	5.17

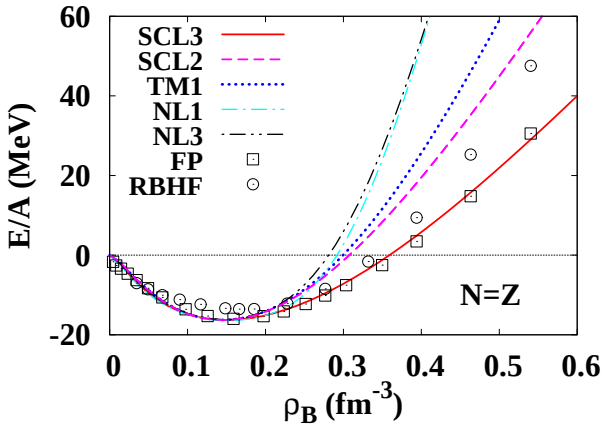

FIG. 3: (Color online) Energy per nucleon in symmetric nuclear matter as a function of the baryon density. Solid, dashed, dotted, dot-dashed, dot-dot-dashed curves show the results in SCL3($m_\sigma = 690$), SCL2 [25], TM1 [41], NL1 [55] and NL3 [56], respectively. Calculated results in variational calculation (FP) [34] and RBHF [40] are also presented by open squares and and open circles, respectively.

Under these assumptions, we have four meson-baryon coupling constants, $g_{\omega N}, g_{\rho N}, g_{\sigma\Lambda}, g_{\zeta\Lambda}$, as model parameters. We have totally six parameters $(m_\sigma, c_\omega, g_{\omega N}, g_{\rho N}, g_{\sigma\Lambda}, g_{\zeta\Lambda})$. For the parameters relevant to normal nuclear properties $(m_\sigma, c_\omega, g_{\omega N}, g_{\rho N})$, first we give m_σ and fix $g_{\omega N}$ and c_ω by fitting the saturation point. Next from the binding energies of Sn and Pb isotopes, m_σ and $g_{\rho N}$ are obtained. The separation energies of Λ hypernuclei mainly reflects the core-Λ potential depth, $U_\Lambda \sim -30$ MeV, thus the combination $g_{\sigma\Lambda}\varphi_\sigma(\rho_0) + g_{\zeta\Lambda}\varphi_\zeta(\rho_0)$ is obtained from this fitting procedure. Finally, the ratio of $g_{\sigma\Lambda}$ and $g_{\zeta\Lambda}$ is determined from the $\Lambda\Lambda$ bond energy in the double Λ hypernucleus. All parameters are tabulated in Table II.

There are two points to be noted in view of the chiral symmetry in the above Lagrangian. We omit pseudoscalar meson effects, and we do not require chiral symmetry in baryon-scalar meson couplings. In discussing the in-medium modification of the chiral condensates, the linear representation is more convenient, where scalar and pseudoscalar mesons appear as chiral partners. In the mean field treatment with parity fixed single particle baryon states, the expectation values of pseudoscalar mesons disappear, and we omit the explicit role of pseudoscalar mesons. Based on the chiral perturbation (ChPT) theory [45] and in the extended relativistic chiral mean field model [46], two pion exchange effects were examined in the relativistic nuclear energy density functional and they would modify the scalar and vector coupling constants in a density dependent way. We here assume that two pion exchange effects are represented in the coupling constants and the self-interaction terms of scalar and vector mesons. In the linear representation, it is possible to construct an SU(3) chiral symmetric Yukawa coupling term of scalar and pseudoscalar mesons with baryons [47], but we have to assume baryons transform as nonet and only D-type coupling appears. For octet baryons having both D- and F-type Yukawa couplings, it is necessary to introduce two-types of baryons [48], or to invoke the non-linear representation [49, 50], which are out of the scope in this paper.

III. FINITE NUCLEI AND NUCLEAR MATTER

A. Nuclear matter and normal nuclei

First we discuss the EOS of symmetric nuclear matter. There are three relevant parameters, m_σ, $g_{\omega N}$ and c_ω. For a given m_σ value, latter two are determined by fitting the saturation point $(\rho_0, E_0/A) = (0.15\ \mathrm{fm}^{-3}, -16.3\ \mathrm{MeV/A})$. In Fig. 3, we show calculated energy per nucleon (E/A) in TM1, SCL2, and the present model (SCL3) with $m_\sigma = 690$ MeV. When we adopt $m_\sigma \sim 700$MeV, the EOS in SCL3 is considerably softer than those in TM1 and SCL2. We also find the SCL3 EOS is in good agreement with the variational calculation results by Friedman and Pandharipande (FP) [34], especially at around ρ_0. SCL3 EOS has rather soft incompressibility $K \sim 211.0$ MeV and this result is comparable with the empirical incompressibility $K = 210 \pm 30$ MeV [51].

Nuclear matter EOS at several ρ_0 has been probed in heavy-ion collisions [52–54]. In Fig. 4, we show the region of pressures consistent with the experimental flow data analyzed by using the Boltzmann equation model [52]. Danielewicz, Lacey and Lynch suggested the range of the incompressibility 167 MeV $\leq K \leq$ 380 MeV in the density range $2\rho_0 \leq \rho_B \leq 5\rho_0$ [52]. Other theoretical model calculations [53, 54] also explain flow data at AGS and SPS energies with $K \simeq 300$ MeV. The calculated pressure in SCL3 is consistent with the pressure range suggested in Ref. [52].

The EOS softening is caused by the ζ meson, which couples with σ through the determinant interaction. In Fig. 2, we show the density dependence of the equilibrium point in $(\varphi_\sigma, \varphi_\zeta)$ plane. Equilibrium values at

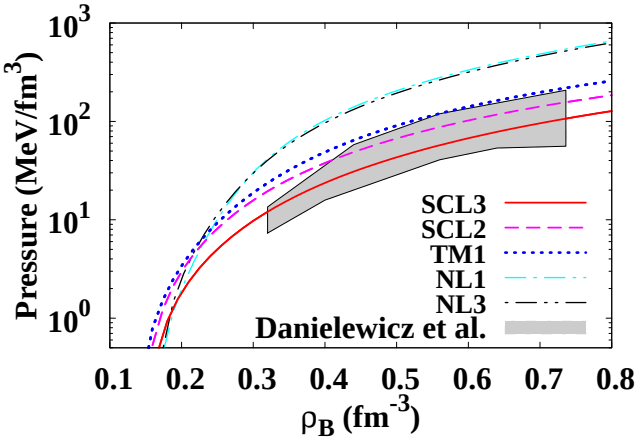

FIG. 4: (Color online) Same as Fig. 3 but for the pressure. Shaded area shows the region of pressures consistent with the experimental flow data analyzed by using the Boltzmann equation model [52].

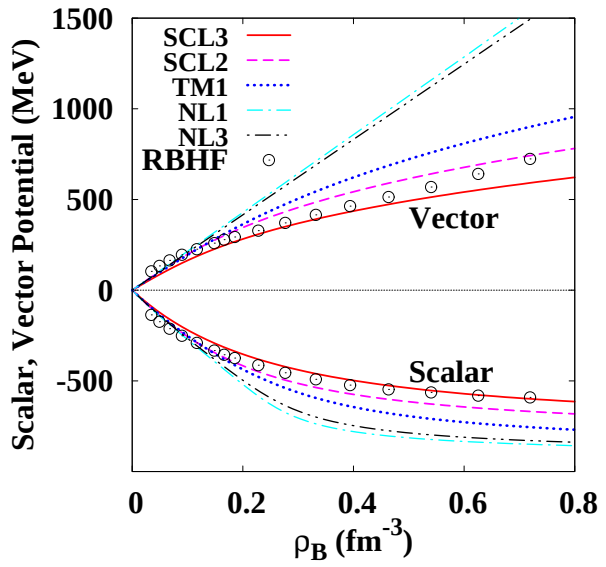

FIG. 5: (Color online) Same as Fig. 3 but for the scalar and vector potentials.

$\rho_B/\rho_0 = 0 \sim 5$ are shown with points. We find that the system evolves along with the valley where ζ values are finite. This ζ variation reduces the quadratic part of the mesonic energy density, while both φ_σ and φ_ζ contribute repulsively in the higher order term, $V_{\sigma\zeta}$. As a result, the energy gain from the scalar mesons is suppressed a little, and it leads to a smaller vector coupling to reproduce the saturation point. Cancellation of smaller scalar and vector potentials leads to a softer EOS in SCL3.

The density dependence of the scalar and vector potentials in SCL3 are found to be qualitatively consistent with the RBHF results [40] at low densities, $\rho_B < 0.3$ fm^{-3}. In Fig. 5, we show the scalar and vector potentials, $U_N^s = M_N^* - M_N = -g_{\sigma N}\varphi_\sigma$ and $U_N^0 = g_{\omega N}\omega$ in symmetric nuclear matter, as functions of density in SCL3 in comparison with those in SCL2, TM1, and RBHF. Scalar and vector potentials grow almost linearly with ρ_B at very low densities, and they are suppressed at higher densities in RBHF via the exchange and correlation, and the relativistic normalization [40]. In RMF models, the suppression is caused by the non-linear terms of σ and ω. The RBHF results lie between SCL2 and SCL3, and the density dependence at $\rho_B < 0.3$ fm^{-3} is well reproduced with SCL3. Once these potentials are given, similar EOSs are obtained at low densities; the difference appears from the non-linear terms, whose residual effects are small at low densities. At high densities ($\rho_B > 0.3$ fm^{-3}), SCL3 gives softer EOS than that in RBHF. This difference may come from the density dependence of the vector potential. As shown in Fig. 5, the vector potential in SCL3 is suppressed more strongly than in RBHF. Since the ω^4 term is introduced to mimic the density dependence in RBHF, it may be necessary to include other types of non-linear interaction terms for vector field provided that the density dependence in RBHF gives the convergent result in the hole-line expansion.

For normal finite nuclei, binding energies per nucleon and charge rms radii are controlled by two parameters, m_σ and $g_{\rho N}$. We determine them by fitting experimental data of binding energies and charge rms radii of some stable nuclei (^{12}C, ^{16}O, ^{40}Ca, ^{48}Ca, ^{58}Ni and ^{90}Zr) and Sn and Pb isotopes. In Fig. 6, we show the calculated binding energies per nucleon (B/A) of C, O, Si, Ca, Ni, Zi, Sn and Pb isotopes, and B/A and charge rms radii for some stable nuclei are shown in Tables III and IV, where we also tabulate NL1 [55], NL3 [56], and non-chiral RMF (TM [22, 41]) results.

From these results, we find that SCL3 RMF model well describes the bulk properties of normal nuclei with the parameters shown in Table II, especially those of Sn and Pb isotopes which we can treat as spherical. Since B/A in these nuclei apparently reflects the character of EOS around ρ_0, our choice of the saturation point and adopted values of parameters ($m_\sigma = 690$MeV, $g_{\rho N} = 4.54$) is appropriate in explaining these data.

B. Λ hypernuclei

From the very early stage [5, 57, 58], RMF models have been applied to Λ hypernuclei. Later, in Ref. [59, 60], tensor type couplings between vector meson and Λ were introduced so as to explain the small ls splitting. This problem was also examined from the view of baryon-meson density dependent coupling [61]. In addition to σ, ω and ρ mesons, hidden strange meson fields (ζ and ϕ) were introduced in order to explain additional hyperon-hyperon interaction [6]. In these works, hyperon-meson coupling constants are determined based on the flavor SU(3) or flavor-spin SU(6) symmetry, Λ hypernuclear single particle energies, hyperon potential depths in nuclear matter, and suggestions from YN g-matrix. In

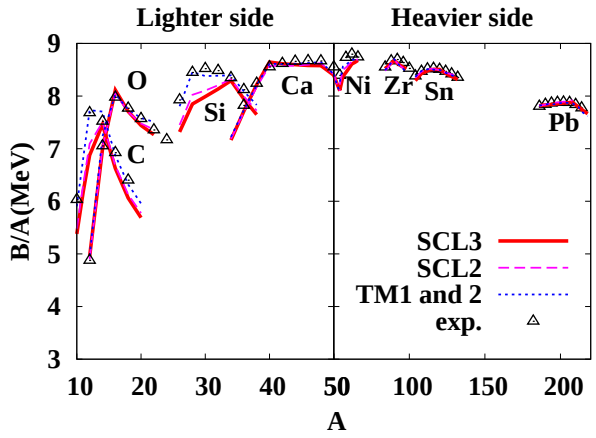

FIG. 6: (Color online) Binding energy per nucleon in normal nuclei from C to Pb isotopes. Solid, dashed and dotted curves show calculated results of SCL3, SCL2, and TM (TM2 for C to Ca isotopes and TM1 for Ni to Pb isotopes) models, respectively. Experimental data are shown in open triangles.

TABLE III: Experimental and theoretical binding energies and of stable nuclei. The results obtained from the SCL3 model are compared with those obtained from TM1, [41] TM2, [41] NL1, [55] NL3, [56] and SCL2 [25] models and with experimental data.

B/A (MeV)							
Nucleus	exp.	SCL3	SCL2	TM1	TM2	NL1	NL3
^{12}C	7.68	6.91	7.09	-	7.68	-	-
^{16}O	7.98	8.11	8.06	-	7.92	7.95	8.05
^{28}Si	8.45	7.85	8.02	-	8.47	8.25	-
^{40}Ca	8.55	8.64	8.57	8.62	8.48	8.56	8.55
^{48}Ca	8.67	8.58	8.62	8.65	8.70	8.60	8.65
^{58}Ni	8.73	8.44	8.54	8.64	-	8.70	8.68
^{90}Zr	8.71	8.67	8.69	8.71	-	8.71	8.70
^{116}Sn	8.52	8.51	8.51	8.53	-	8.52	8.51
^{196}Pb	7.87	7.84	7.87	7.87	-	7.89	-
^{208}Pb	7.87	7.87	7.87	7.87	-	7.89	7.88

Refs. [57, 58], $x \equiv g_{\sigma\Lambda}/g_{\sigma N} \simeq g_{\omega\Lambda}/g_{\omega N} \simeq 1/3$ is adopted from discussions of π, ρ and ω exchanges [57] or by fitting single particle levels of Λ hypernuclei [58], while in Ref. [5], the ratio is set to be $x = 2/3$ from light quark counting arguments. In Refs. [6, 60], the vector meson-hyperon couplings are fixed from the SU(6) relation or the additive quark model results, *e.g.* $g_{\omega\Lambda} = g_{\omega\Sigma} = 2g_{\omega\Lambda} = 2/3g_{\omega N}$, while the scalar meson-hyperon couplings are determined from the Λ hypernuclear single particle energies or the hyperon potential depths in baryonic matter. In Ref. [59], several sets of parameters are compared in the range $g_{\omega\Lambda}/g_{\omega N} = 0.18 - 0.63$, and it is concluded that the Λ single particle energies are not enough to determine the meson-Λ coupling constants.

Since the experimental information on YN interaction

TABLE IV: Same as Table III but for charge rms radii.

charge rms radius (fm)							
Nucleus	exp.	SCL3	SCL2	TM1	TM2	NL1	NL3
^{12}C	2.46	2.47	2.43	-	2.39	-	-
^{16}O	2.74	2.63	2.62	-	2.67	2.74	2.73
^{28}Si	3.09	3.06	3.04	-	3.07	3.03	-
^{40}Ca	3.45	3.43	3.44	3.44	3.50	3.48	3.47
^{48}Ca	3.45	3.46	3.46	3.45	3.50	3.44	3.47
^{58}Ni	3.77	3.78	3.77	3.76	-	3.73	3.74
^{90}Zr	4.26	4.26	4.27	4.27	-	4.27	4.29
^{116}Sn	4.63	4.61	4.62	4.61	-	4.61	4.61
^{196}Pb	-	5.48	5.48	5.47	-	5.47	-
^{208}Pb	5.50	5.54	5.54	5.53	-	5.57	5.58

is limited, it is valuable to study the hypernuclear systems with the RMF models including the chiral potential which can explain normal nuclear property. In previous studies [47, 49], chiral SU(3) symmetric RMF models are proposed. In the linear [47] and non-linear [49] representation, various types of meson Lagrangian are compared. These models describe the normal nuclear properties very well [49, 50], while the hypernuclear properties in these models are not satisfactory from a phenomenological point of view. Especially Σ and Ξ hyperons are considered to feel repulsive [62] and weakly attractive [63] potentials, but these features are not explained yet. This may be suggesting the importance of other types of meson-hyperon couplings other than the Yukawa coupling or the SU$_f$(3) breaking effects.

In the present work, we study single- and double-Λ hypernuclei in the SCL3 RMF model, which has already shown to work well in normal nuclei and nuclear matter as demonstrated in the previous subsection. We adopt the SU$_f$(3) relation for vector coupling, and scalar meson-Λ Yukawa coupling constants are chosen to fit the Λ separation energies of single Λ hypernuclei and the $\Lambda\Lambda$ bond energy in ${}^{6}_{\Lambda\Lambda}$He. In this treatment, the scalar meson-Λ coupling terms do not necessarily preserve the chiral SU(3) symmetry, but this may be an appropriate prescription at present because of the phenomenological problems in the chiral SU(3) RMF mentioned above. We omit the vector meson-hyperon tensor couplings, which does not affect the EOS in the mean field treatment.

In single- and double-Λ hypernuclei, we have four adjustable parameters, $g_{\sigma\Lambda}$, $g_{\zeta\Lambda}$, $g_{\omega\Lambda}$ and $g_{\phi\Lambda}$. Here, we assume that the vector couplings obey the lowest order SU$_f$(3) symmetric relation [15, 42],

$$\begin{aligned}\mathcal{L}_{\rm BV} &= \sqrt{2}\{g_s\,{\rm tr}\,(M_v)\,{\rm tr}\,(\bar{B}B) + g_D\,{\rm tr}\,(\bar{B}\,\{M_v, B\}) \\ &\quad + g_F\,{\rm tr}\,(\bar{B}\,[M_v, B])\} \\ &= \sqrt{2}\{g_s\,{\rm tr}\,(M_v)\,{\rm tr}\,(\bar{B}B) + g_1\,{\rm tr}\,(\bar{B}M_vB) \\ &\quad + g_2\,{\rm tr}\,(\bar{B}BM_v)\}\ , \end{aligned} \tag{30}$$

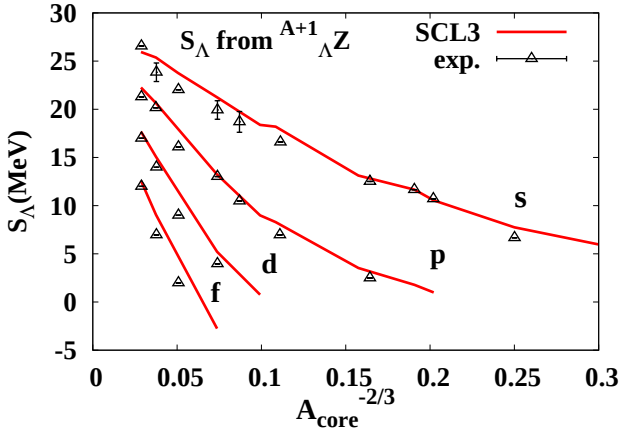

FIG. 7: (Color online) Separation energy of Λ.Parameters are determined by fitting S_Λ of $^{13}_{\Lambda}$C and $^{12}_{\Lambda}$C. S_Λ of p, d and f are wait-averaged considering the state numbers in each levels.

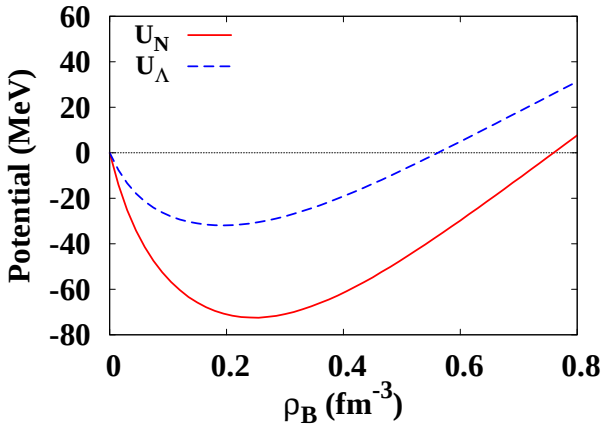

FIG. 8: (Color online) Single particle potential of nucleon and Λ. Solid and dashed curves show the potential of nucleon and Λ, respectively.

where $g_D = (g_1+g_2)/2$, $g_F = (g_1-g_2)/2$, and the Lorentz indices and gamma matrices are assumed. In this form of vector coupling, $g_{\omega\Lambda}$ and $g_{\phi\Lambda}$ are already fixed by the vector coupling constants with nucleons, $g_{\omega N}$ and $g_{\rho N}$, as

$$g_{\omega\Lambda} = \frac{5}{6} g_{\omega N} - \frac{1}{2} g_{\rho N}, \quad g_{\phi\Lambda} = \frac{\sqrt{2}}{6} \left(g_{\omega N} + 3 g_{\rho N} \right) \ . \quad (31)$$

Scalar coupling constants, $g_{\sigma\Lambda}$ and $g_{\zeta\Lambda}$, are then tuned to reproduce existing data of S_Λ and the ΛΛ bond energy, $\Delta B_{\Lambda\Lambda}$, observed in the Nagara event, $^{6}_{\Lambda\Lambda}$He [19].

In Fig. 7, we show the calculated results of S_Λ with the parameter set in Table II. Here, we evaluate the zero-point kinetic energy, $E_{\rm ZPE}$, with a harmonic-oscillator wave function as $E_{\rm ZPE} = \frac{3}{4} \cdot 41 A_{\rm core}^{-1/3}$ MeV. The results of the S_Λ for p, d and f levels are the weight-averaged ones of the spin-orbit partners.

The scalar potential of Λ is given in the form of linear combination of the coupling constants and chiral condensates,

$$U_\Lambda^s(\rho_B) = -[g_{\sigma\Lambda}\varphi_\sigma(\rho_B) + g_{\zeta\Lambda}\varphi_\zeta(\rho_B)] \ . \quad (32)$$

In Fig. 8, we show the single particle potential for Λ, defined as the sum of the scalar and vector potentials, $U_\Lambda = U_\Lambda^s + U_\Lambda^0$, where the temporal component of the vector potential U_Λ^0 is defined in Eq. (29). This sum roughly corresponds to the Schrödinger equivalent potential for Λ, $U_\Lambda^{\rm (SEP)} = U_\Lambda^s + (E/M_\Lambda) U_\Lambda^0$. As in the previous studies [15–17], U_Λ amounts to be around −30 MeV at ρ_0. Calculated S_Λ values are very similar as far as the scalar potentials at ρ_0 are the same.

The ls splitting between $p^\Lambda_{1/2}$ and $p^\Lambda_{3/2}$ in $^{13}_{\Lambda}$C is calculated to be 900 keV in the present treatment. This result is larger than the observed small ls splitting [64]. A small ls splitting would be obtained by including the tensor type couplings between meson and Λ hyperon [59], since this coupling directly corresponds to ls force when we translate the Dirac equation in RMF into a Schrödinger equivalent form. This coupling, however, reduces only the ls splitting and does not change the average location of ls partners. Thus, we suppose that determined $g_{\sigma\Lambda}$ and $g_{\zeta\Lambda}$ are not affected dramatically. Two pion exchange anti-ls force is also suggested as the origin of the small ls splitting and examined by introducing density dependent coupling between meson and baryon [61] and in the in-medium chiral SU(3) dynamics [65].

In Fig. 9, we show the relation of $g_{\sigma\Lambda}$ and $g_{\zeta\Lambda}$ determined by fitting S_Λ of $^{12}_{\Lambda}$C and $^{13}_{\Lambda}$C. This relation is roughly evaluated as $\widetilde{g}_{\sigma\Lambda} = g_{\sigma\Lambda} + g_{\zeta\Lambda}/2 \simeq 6$. All the parameter sets on the solid line can reproduce S_Λ of various single Λ hypernuclei similarly to the one shown in Fig. 7. We also examine $\Delta B_{\Lambda\Lambda}$ in this parameter plane and find that the parameter sets in the gray shaded area explain the experimental $\Delta B_{\Lambda\Lambda}$ value of $^{6}_{\Lambda\Lambda}$He within the error. Combining these results, we obtain the set of coupling constants as $(g_{\sigma\Lambda}, g_{\zeta\Lambda}) = (3.40, 5.17)$ shown in Table II, which explains S_Λ and the central value of the experimental bond energy ($\Delta B_{\Lambda\Lambda}$) simultaneously.

The above set of coupling constants $(g_{\sigma\Lambda}, g_{\zeta\Lambda})$ deviates from a naive estimate, $g_{\sigma\Lambda}/g_{\sigma N} = 2/3$ and $g_{\sigma\Lambda}/g_{\zeta\Lambda} = \sqrt{2}$. While the σΛ coupling is small, the scalar potential for Λ is around 2/3 of that for nucleons, and it is still dominated by σ. The additional scalar potential comes from ζ, which does not couple with nucleons directly but appears from the σζ mixing generated by the KMT term in the Lagrangian. Since φ_ζ evolves as $\varphi_\zeta \simeq \varphi_\sigma/2$ in symmetric nuclear matter as seen in Fig. 2, the scalar potential of Λ behaves as $U_\Lambda^s \simeq -\widetilde{g}_{\sigma\Lambda}\,\varphi_\sigma$. The effective coupling $\widetilde{g}_{\sigma\Lambda}$ is around 2/3 of $g_{\sigma N}$, then the smaller Λ scalar potential from σ is compensated by the ζ meson. The obtained $g_{\sigma\Lambda}$ is close to 1/3 of $g_{\sigma N}$, as suggested from the two pion exchange [57]. These observations may be suggesting the importance of pions and KMT term at finite densities.

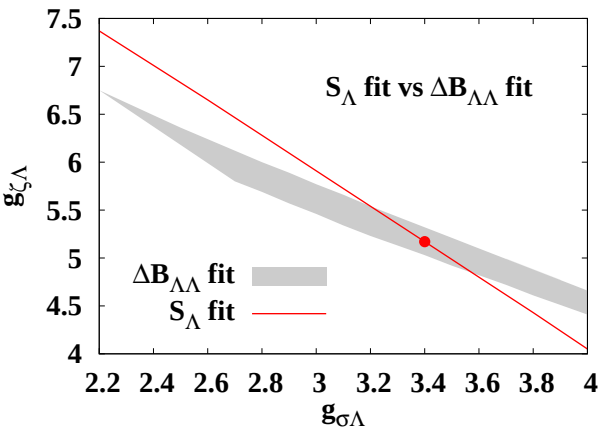

FIG. 9: (Color online) $g_{\sigma\Lambda}$ and $g_{\zeta\Lambda}$ suggested from experimental data. Solid line shows the relation between $g_{\sigma\Lambda}$ and $g_{\zeta\Lambda}$ determined by fitting S_Λ of ${}^{12}_{\Lambda}$C and ${}^{13}_{\Lambda}$C, and gray shaded area shows the region which explains the experimental $\Delta B_{\Lambda\Lambda}$ value of ${}^{6}_{\Lambda\Lambda}$He within the error. The filled point represents the pair of $g_{\sigma\Lambda}$ and $g_{\zeta\Lambda}$, which explains S_Λ and the central value of the experimental bond energy ($\Delta B_{\Lambda\Lambda}$) simultaneously, and is adopted in the present work.

C. Neutron star matter

In previous subsections, we have fixed all parameters for nucleon and Λ by fitting the empirical saturation point of symmetric nuclear matter, and the binding energies of normal nuclei and Λ hypernuclei. Now we apply the SCL3 RMF model to neutron star (NS) matter.

In NS matter, we require neutrinoless β–equilibrium and charge neutrality condition,

$$\mu_i = b_i\mu_B - q_i\mu_e \ , \tag{33}$$

$$\rho_c = \sum_B q_B\rho_v^{(B)} + \sum_l q_l\rho_v^{(l)} = 0 \ . \tag{34}$$

The first equation relate the chemical potentials as, $\mu_n = \mu_p + \mu_e = \mu_\Lambda$ and $\mu_e = \mu_\mu$. Under this equilibrium condition, we calculate the energy density (ε) and pressure (P), and we solve the Tolman–Oppenheimer–Volkoff(TOV) equation,

$$\frac{dP}{dr} = -\frac{[P(r)+\varepsilon(r)][M(r)+4\pi r^3P(r)]}{r(r-2M(r))} \ . \tag{35}$$

where $M(r)$ denotes the mass inside the radius r. Here, we neglect nuclear crust for simplicity.

In Fig. 10, we show the NS matter EOS. We compare the results of SCL3 RMF model only with nucleons (SCL3) and with Λ hyperons (SCL3Λ). We also show the NS matter EOS in SCL2 [25], TM1 [41], NL1 [55], NL3 [56] and IOTSY [10], where Λ hyperons are not taken into account except for IOTSY. The IOTSY RMF model is based on TM1 model and includes all octet hyperons (Λ, Σ, Ξ). We find that the NS matter EOS in SCL3 is softer than those in other RMF EOSs without hyperons. Especially, when we include Λ, Λ hyperons appear at around $2\rho_0$ and NS matter EOS including Λ hyperons becomes further softer.

In Fig. 11, we show the results of neutron star mass as a function of the central density with SCL3, SCL3Λ, SCL2, TM1, IOTSY, NL1 and NL3 models. While the EOS in SCL3 is much softer than other EOSs, calculated maximum NS mass in SCL3 (without hyperon) is $1.65M_\odot$, which exceeds the precisely observed NS mass, 1.44 $M_\odot$ [66]. When Λ hyperons are included, the maximum mass is calculated to be $1.40M_\odot$ with SCL3Λ and underestimates the observed mass.

This underestimate is caused by the softer EOS, particularly in the high ρ_B region. It is suggested that extra repulsion coming from three-baryon interactions or string-junction model [67] which are repulsive for all baryon universally are needed to surpass the known NS mass data in non-relativistic calculations [36, 37, 68]. In RMF models, the EOS of nuclear matter is stiff enough, and extra repulsion is not generally required to support 1.44 $M_\odot$. In SCL3 and SCL3Λ, however, the incompressibility is as small as the empirical value and the pressure at high density region is compatible with the estimate in heavy-ion collisions [52]. Thus, we encounter the same problem as in the non-relativistic calculations and have to consider additional repulsions which have a large effect at high densities. One of the candidates of this extra repulsion may come from the $\sigma\omega$ coupling, such as in the term of $\sigma^2\omega^2$ [28, 69]. The $\sigma\omega$ coupling results in reducing of the vector meson mass at high densities, and is found to give very stiff EOS when combined with the linear σ model. Inclusion of such coupling may stiffen EOS in high ρ_B region after re-fitting experimental data and it may solve the underestimation of the maximum mass of NS.

Now we examine the effects of Σ hyperons in neutron star matter. In neutron star matter, it was believed that the Σ^- baryon would appear at the lowest density among the hyperons provided that the potential for Σ baryons in symmetric nuclear matter is similar to that for Λ [5, 6]. The strength of Σ-nucleus optical potential have been studied from the atomic shifts of Σ^- [70, 71], which is sensitive to the attraction in Σ^--nucleus potential at nuclear surface. In the inner region of nuclei, the analysis of the Σ^- quasi free production spectra from (π^-, K^+) and (K^-, π^+) reactions have yielded that repulsive Σ-nucleus potential is favored [62]. From these point of view, we employ the repulsive Σ potential [74] which is suggested from $\mathrm{SU}_f(3)$ relation, Eq. (30). Coupling constants, $g_{\omega\Sigma}$ and $g_{\phi\Sigma}$ are given as

$$g_{\omega\Sigma} = \frac{1}{2}\left(g_{\omega N} + g_{\rho N}\right), \ g_{\phi\Sigma} = \frac{\sqrt{2}}{2}\left(g_{\omega N} - g_{\rho N}\right). \tag{36}$$

From the $\mathrm{SU}_f(3)$ relation, $g_{\rho\Sigma}$ should be equal to $g_{\omega\Sigma}$,

$$g_{\rho\Sigma}^{\mathrm{SU}(3)} = g_{\omega\Sigma} \simeq 2g_{\rho N} \ . \tag{37}$$

In order to explain the atomic shift data of Σ^-, however, we need to adopt a smaller value of $g_{\rho\Sigma}$. In an

RMF model fit, Mares *et al.* showed that both of Si and Pb atomic shift data [75] are well explained by adopting $g_{\rho\Sigma}/g_{\rho N} \simeq 2/3$ [71]. With the present Lagrangian, we have fitted the Σ^- atomic shift data and have obtained the values $g_{\rho\Sigma} = 1.97$ ($g_{\rho\Sigma}/g_{\rho N} = 0.434$) and $g_{\sigma\Sigma} = 3.16$ under the assumption of the naïve quark counting coupling ratio for σ and ζ, $g_{\sigma\Sigma} = \sqrt{2}g_{\zeta\Sigma}$. The calculated EOS, mass of neutron star, and particle fraction $Y_i = \rho_i/\rho_B$ with Σ hyperons are shown in Figs. 10, 11, and in the middle panel of Fig. 12, respectively. In neutron star matter, Σ^- starts to emerge around $\rho_B \sim 0.4$ as a substitute of leptons because of its negative charge. Other Σ hyperons (Σ^0, Σ^+) do not appear even at $10\rho_0$ because of the repulsive potential and the negative charge chemical potential. The calculated EOS and maximum mass of neutron star are not affected much. The repulsive potential suppresses the effects of Σ baryons compared to those of Λ, which plays a decisive role as a substitute of the dominant component, n.

It is interesting to find that the starting density of Σ^- hyperon ($\rho_B \simeq 0.4$ fm^{-3}) is much lower than those in previous studies [7–10], which also adopt repulsive Σ potential in symmetric nuclear matter. In these works, Σ^- appears at much higher density. The main difference in the present work is the coupling strength with the ρ meson. In Refs. [9, 10], the SU(3) value ($g_{\rho\Sigma}/g_{\rho N} = 2$) is adopted and the repulsive interaction from ρ is strong in high density neutron star matter, while the present coupling ($g_{\rho\Sigma}/g_{\rho N} = 0.434$) is much smaller and the repulsive potential from ρ is weaker. In order to demonstrate this point, we show the particle fraction results with $g_{\rho\Sigma}/g_{\rho N} = 2$ in the right panel of Fig. 12. We find that Σ^- appears only at $\rho_B \gtrsim 1$ fm^{-3}, which is qualitatively consistent with previous works [7–10],

One of the problems in the present SCL3 is that the c_ω value ($c_\omega = 294.9$) is larger than those in TM1 ($c_\omega = 71.3075$) and SCL2 ($c_\omega = 200$) models. The potential term of $c_\omega\omega^4/4$ strongly suppresses ω meson field especially at high ρ_B [41]. The lower c_ω value an RMF model has, the higher neutron star maximum mass the EOS shows as seen in Figs. 10 and 11. When we reduce this parameter by changing m_σ value and re-fixing all the parameter in the way as we discussed, calculated maximum mass of neutron star should be 1.8 $M_\odot$ on the condition of $m_\sigma = 725$MeV and $c_\omega = 75.66$. With this choice, however, we cannot reproduce the binding energies of Sn and Pb isotopes. Thus, in addition to chiral potential, the form and strength of vector meson potential is also important and should be investigated further.

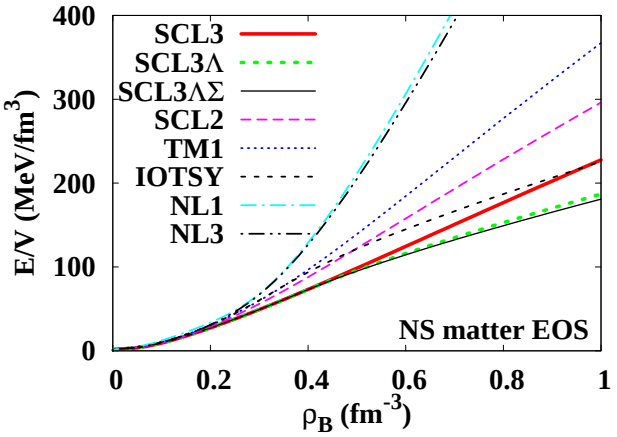

FIG. 10: (Color online) Energy per baryon in neutron star matter. Solid, short-dashed, bold-dashed, dotted, thin-dashed, dot-dashed, dot-dot-dashed curves show the results of SCL3, SCL3Λ, SCL2, TM1, IOTSY, NL1 and NL3 results, respectively.

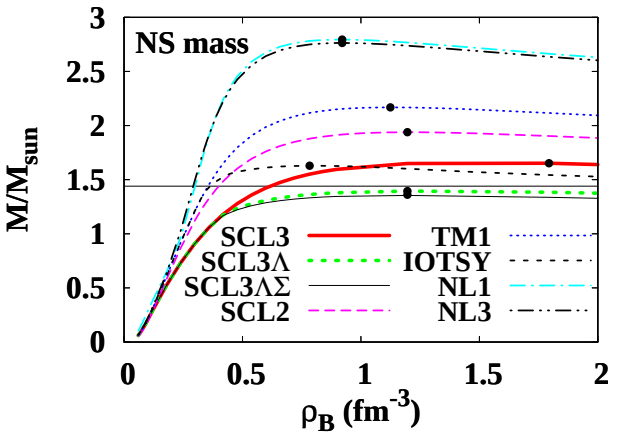

FIG. 11: (Color online) Same as Fig. 10 but for the neutron star mass as a function of the central density.

IV. SUMMARY AND DISCUSSION

In this paper, we have proposed a chiral SU(3) symmetric RMF (SCL3 RMF) model, and examined its properties in nuclear matter, normal nuclei, Λ hypernuclei and neutron star matter. We adopt a logarithmic chiral SU(3) potential, as the energy density as a function of σ at $\rho_B = 0$, derived in the strong coupling limit of lattice QCD [26]. The Kobayashi-Maskawa-'t Hooft (KMT) determinant interaction term [32, 33] is also introduced in order to take account of the U$_A$(1) anomaly. Since the chiral symmetry relates the condensates and hadron masses, the number of parameters are reduced by introducing this symmetry. After fitting $\pi, K,$ f$_0$(980) masses together with f_π and f_ζ, we have only one free parameter, m_σ, in the vacuum part. Under the assumptions that the nucleon mass are fully generated by the chiral condensate ($M_N = g_{\sigma N} f_\pi$) and that the nucleon does not couple with $\bar{s}s$ mesons, we determine four parameters relevant to normal nuclei ($m_\sigma, g_{\omega N}, g_{\rho N}, c_\omega$), by fitting the empirical and experimental data of symmetric nuclear matter saturation point, binding energies and size of normal nuclei. For Λ hypernuclei, we assume that the vector couplings obey the lowest order SU$_f$(3) symmetric relation [15, 42],

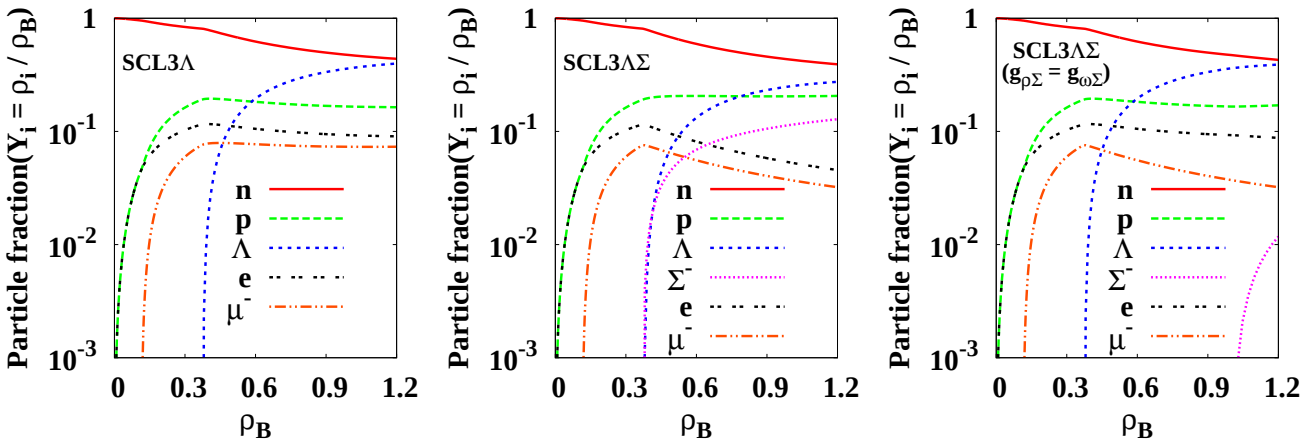

FIG. 12: (Color online) Calculated particle fraction Y_i of n, p, Λ, Σ^-, e^-, and μ^-. The other Σ hyperons (Σ^0 and Σ^+) do not emerge in this baryon density range.

and the remaining two parameters ($g_{\sigma\Lambda}, g_{\zeta\Lambda}$) are determined by fitting the experimental data of the separation energies of single-Λ hypernuclei and the $\Lambda\Lambda$ bond energy in the double-Λ hypernucleus, ${}^{6}_{\Lambda\Lambda}$He.

We find that the SCL3 model well describes the symmetric nuclear matter properties and the bulk properties of normal nuclei: The equation of state (EOS) is found to be softened by the $\sigma\zeta$ coupling generated by the KMT interaction, and the incompressibility of symmetric nuclear matter is found to be $K \simeq 210$ MeV, which is consistent with the empirical value, $K = 210 \pm 30$ MeV [51]. The EOS around ρ_0 is in agreement with the results of variational calculations [34], and the pressure in the density region of $2\rho_0 \leq \rho_B \leq 5\rho_0$ is in agreement with the estimates from heavy-ion collision data [52]. The density dependence of the vector potential is close to that in the relativistic Brückner-Hartree-Fock (RBHF) calculation [40] at low densities, $\rho_B < 3\rho_0$. The binding energies of normal nuclei from C to Pb isotopes are reasonably well explained except for the $jj-$closed shell nuclei. Single- and double-Λ hypernuclei are also well described. Separation energies of Λ in single-Λ hypernuclei, S_Λ, are mainly determined by the potential depth, and the $\Lambda\Lambda$ bond energy depends on the $\zeta\Lambda$ coupling $g_{\zeta\Lambda}$ more strongly than on the $\sigma\Lambda$ coupling $g_{\sigma\Lambda}$.

The calculated maximum neutron star mass in the present SCL3 RMF model underestimates the observed neutron star mass $1.44M_\odot$. This underestimate would originate from the soft EOS of nuclear matter at high densities. The vector potential is suppressed more strongly from the linear behavior, $\omega \sim g_{\omega N}\rho_B/m_\omega^2$, than the RBHF results, and the EOS of symmetric matter is softer than the results in the variational calculation [34] and RBHF [34] at high densities. The suppression of the vector potential is caused by the ω self-interaction term, $-c_\omega\omega^4/4$, whose coefficient is large in SCL3 compared with previous RMF models with this term. Since this term is introduced phenomenologically to simulate the suppression of the vector potential in RBHF [41], it would be necessary to introduce other types of coupling, such as the scalar meson-vector meson coupling, $\sigma^2\omega^2$ [28, 69]. The scalar-vector coupling acts to modify the in-medium vector meson mass [21, 72]. It may be interesting to invoke the results of strong coupling lattice QCD with finite coupling effects, where the plaquette contribution is found to generate the vector potential [73]. Another possibility is to introduce the repulsive three-baryon force, which is widely adopted in non-relativistic theories [34–37].

In this paper, we examine how Λ and Σ hyperons affect the neutron star matter EOS based on experimental data. The isospin dependence of Σ potential in nuclear matter is found to be important for the composition at high densities. Ξ hyperons are not included because the data are not enough to constrain the potential [63]. Since Ξ hyperons may further soften EOS at high densities, it is necessary to find the mechanism of re-stiffening at high densities in order to construct reliable and chiral SU(3) symmetric EOS including all these hyperons. Explicit role of pions [45, 46, 76] is another important subject to study in terms of relativistic nuclear many-body problems. The ls-like potential [65, 77] from pion exchange would improve the binding energies of jj-closed shell nuclei. In addition, tensor suppression may be play a critical role in EOS at higher densities.

Acknowledgments

We would like to thank Professor Avraham Gal and Jiri Mares for useful discussions. This work was supported in part by KAKENHI from MEXT and JSPS under the grant numbers, 17070002, 19540252 and 20·4326, Global COE Program "The Next Generation of Physics, Spun from Universality and Emergence", and the Yukawa International Program for Quark-hadron Sci-

ences (YIPQS). Discussions during the YIPQS international workshop on "New Frontiers in QCD 2010", were useful to complete this work.

Appendix A: The masses of scalar and pseudoscalar mesons

We show the formulae of the scalar and pseudoscalar meson masses except for σ, ζ, π and K, which we have already shown in Sec. II. When we adopt expectation value of each mesons and mass values of π, K and f_0 as constraints, mass of a_0, η and η' can be represented as a function of parameter m_σ. These masses can be read as

$$m_{a_0}^2 = b' + \frac{2a'}{f_\pi^2} + 2d' f_\zeta \tag{A1}$$

$$m_\kappa^2 = b' + \frac{\sqrt{2}a'}{f_\pi f_\zeta'} + \sqrt{2}d' f_\pi \ , \tag{A2}$$

$$m_\eta^2 = b' - \frac{2a'}{f_\pi^2} + 2d' f_\zeta \ , \tag{A3}$$

$$m_{\eta_s}^2 = b' - \frac{a'}{f_\zeta'^2} \ , \tag{A4}$$

$$\xi_{\eta\eta_s} = 2d' f_\pi \ , \tag{A5}$$

$$M_\eta^2 = \frac{\left(m_\eta^2 + m_{\eta_s}^2\right) - \sqrt{\left(m_\eta^2 - m_{\eta_s}^2\right)^2 + 4\xi_{\eta\eta_s}^2}}{2} \ , \tag{A6}$$

$$M_{\eta'}^2 = \frac{\left(m_\eta^2 + m_{\eta_s}^2\right) + \sqrt{\left(m_\eta^2 - m_{\eta_s}^2\right)^2 + 4\xi_{\eta\eta_s}^2}}{2} \ . \tag{A7}$$

where we use same parameters, such as a', b' and d', defined in Sec. II. We have the mixing term of η and η_s mesons, thus one have to diagonalize their mass matrix to obtain vacuum masses. We tabulate calculated masses as functions of m_σ in Table I.

[1] J. M. Lattimer and F. D. Swesty, Nucl. Phys. **A535**, 331 (1991).
[2] H. Shen, H. Toki, K. Oyamatsu and K. Sumiyoshi, Nucl. Phys. **A637**, 435 (1998).
[3] M. Lutz, Nucl. Phys. **A642**, 171 (1998).
[4] A. R. Bodmer, Phys. Rev. D **4**, 1601 (1971); E. Witten, Phys. Rev. D **30**, 272 (1984); A. Gal and C. B. Dover, Nucl. Phys. **A585**, 1C (1995); N. K. Glendenning and J. Schaffner-Bielich, Phys. Rev. C **58**, 1298 (1998); I. Bednarek and R. Manka, J. Phys. G **31**, 1009 (2005).
[5] N. K. Glendenning, Phys. Rev. C **23**, 2757 (1981); Phys. Lett. B **114**, 392 (1982); Astrophys. J. **293**, 470 (1985).
[6] J. Schaffner, C. B. Dover, A. Gal, C. Greiner and H. Stoecker, Phys. Rev. Lett. **71**, 1328 (1993); J. Schaffner, C. B. Dover, A. Gal, C. Greiner, D. J. Millener and H. Stoecker, Annals Phys. **235**, 35 (1994); J. Schaffner and I. N. Mishustin, Phys. Rev. C **53**, 1416 (1996).
[7] S. Balberg and A. Gal, Nucl. Phys. A **625**, 435 (1997).
[8] P. K. Sahu and A. Ohnishi, Nucl. Phys. A **691**, 439 (2001).
[9] J. Schaffner-Bielich, Nucl. Phys. A **804**, 309 (2008).
[10] C. Ishizuka, A. Ohnishi, K. Tsubakihara, K. Sumiyoshi and S. Yamada, J. Phys. G **35**, 085201 (2008).
[11] N. K. Glendenning and J. Schaffner-Bielich, Phys. Rev. Lett. **81**, 4564 (1998).
[12] A. Ohnishi, D. Jido, T. Sekihara and K. Tsubakihara, Phys. Rev. C **80**, 038202 (2009).
[13] A. K. Holme, E. F. Staubo, L. P. Csernai, E. Osnes and D. Strottman, Phys. Rev. D **40**, 3735 (1989).
[14] R. D. Pisarski and D. H. Rischke, Phys. Rev. Lett. **83**, 37 (1999).
[15] C. B. Dover and A. Gal, Prog. Part. Nucl. Phys. **12**, 171 (1985).
[16] D. J. Millener, C. B. Dover and A. Gal, Phys. Rev. C **38**, 2700 (1988).
[17] H. Bando, T. Motoba and J. Zofka, Int. J. Mod. Phys. A **5** (1990) 4021.
[18] R. E. Chrien [BNL (PI+, K+) Collaboration], Nucl. Phys. **A478**, 705c (1988); P. H. Pile *et al.*, Phys. Rev. Lett. **66**, 2585 (1991); T. Hasegawa *et al.*, Phys. Rev. C **53**, 1210 (1996); O. Hashimoto and H. Tamura, Prog. Part. Nucl. Phys. **57**, 564 (2006).
[19] H. Takahashi *et al.*, Phys. Rev. Lett. **87**, 212502 (2001).
[20] Y. Nambu and G. Jona-Lasinio, Phys. Rev. **122**, 345 (1961); Phys. Rev. **124**, 246 (1961).
[21] T. Hatsuda and T. Kunihiro, Phys. Rept. **247**, 221 (1994).

[22] A. Hosaka and H. Toki, *Singapore, Singapore: World Scientific (2001) 379 p* and references therein.

[23] K. Sumiyoshi, H. Suzuki, S. Yamada and H. Toki, Nucl. Phys. **A730**, 227 (2004).

[24] S. Tsuruta, M. A. Teter, T. Takatsuka, T. Tatsumi and R. Tamagaki, Astrophys. J. **571**, L143 (2002).

[25] K. Tsubakihara and A. Ohnishi, Prog. Theor. Phys. **117**, 903 (2007).

[26] N. Kawamoto and J. Smit, Nucl. Phys. **B190**, 100 (1981); H. Kluberg-Stern, A. Morel, O. Napoly and B. Petersson, Nucl. Phys. B **190**, 504 (1981).

[27] P. H. Damgaard, N. Kawamoto and K. Shigemoto, Phys. Rev. Lett. **53**, 2211 (1984); E. M. Ilgenfritz and J. Kripfganz, Z. Phys. C **29**, 79 (1985); P. H. Damgaard, N. Kawamoto and K. Shigemoto, Nucl. Phys. **B264** (1986), 1; N. Bilic, K. Demeterfi and B. Petersson, Nucl. Phys. **B377** (1992), 651; Y. Nishida, K. Fukushima and T. Hatsuda, Phys. Rept. **398** (2004), 281; Y. Nishida, Phys. Rev. D **69**, 094501 (2004); K. Fukushima, Prog. Theor. Phys. Suppl. **153**, 204 (2004); X. Q. Luo, Phys. Rev. D **70** (2004), 091504(R); N. Kawamoto, K. Miura, A. Ohnishi and T. Ohnuma, Phys. Rev. D **75**, 014502 (2007).

[28] J. Boguta, Phys. Lett. **B120**, 34 (1983); Phys. Lett. **B128**, 19 (1983).

[29] T. D. Lee and G. C. Wick, Phys. Rev. D **9**, 2291 (1974).

[30] T. Matsui and B. D. Serot, Ann. Phys. **144**, 107 (1982); P. Sahu and A. Ohnishi, Prog. Theor. Phys. **104**, 1163 (2000).

[31] Y. Ogawa H. Toki, S. Tamenaga, H. Shen, A. Hosaka, S. Sugimoto and K. Ikeda, Prog. Theor. Phys. **111**, 75 (2004).

[32] M. Kobayashi and T. Maskawa, Prog. Theor. Phys. **44**, 1422 (1970). M. Kobayashi, H. Kondo and T. Maskawa, Prog. Theor. Phys. **45**, 1955 (1971).

[33] G. 't Hooft, Phys. Rev. D **14**, 3432 (1976) [Erratum-ibid. D **18**, 2199 (1978)]; G. 't Hooft, Phys. Rept. **142**, 357 (1986).

[34] B. Friedman and V. R. Pandharipande, Nucl. Phys. **A361**, 502 (1981).

[35] A. Akmal, V. R. Pandharipande and D. G. Ravenhall, Phys. Rev. C **58**, 1804 (1998).

[36] S. Nishizaki, T. Takatsuka and Y. Yamamoto, Prog. Theor. Phys. **108**, 703 (2002).

[37] M. Baldo, G. F. Burgio and H. J. Schulze, Phys. Rev. C **61**, 055801 (2000).

[38] I. Vidana, A. Polls, A. Ramos, L. Engvik and M. Hjorth-Jensen, Phys. Rev. C **62**, 035801 (2000).

[39] H. J. Schulze, A. Polls, A. Ramos and I. Vidana, Phys. Rev. C **73**, 058801 (2006).

[40] R. Brockmann and R. Machleidt, Phys. Rev. C **42**, 1965 (1990); R. Brockmann and H. Toki, Phys. Rev. Lett. **68**, 3408 (1992).

[41] Y. Sugahara and H. Toki, Nucl. Phys. **A579**, 557 (1994).

[42] U. G. Meissner, Rept. Prog. Phys. **56**, 903 (1993).

[43] S. Okubo, Phys. Lett. **5**, 165 (1963); G. Zweig, *Developments in the Quark Theory of Hadrons* (Hadronic Press, Massachusetts, 1980); J. Iizuka, Prog. Theor. Phys. Suppl. **37**, (1966) 38; J. Iizuka, Prog. Theor. Phys. Suppl. **37**, 21 (1966).

[44] N. Isgur and H. B. Thacker, Phys. Rev. D **64**, 094507 (2001).

[45] P. Finelli, N. Kaiser, D. Vretenar and W. Weise, Nucl. Phys. A **770**, 1 (2006).

[46] J. Hu, Y. Ogawa, H. Toki, A. Hosaka and H. Shen, Phys. Rev. C **79**, 024305 (2009).

[47] P. Papazoglou, S. Schramm, J. Schaffner-Bielich, H. Stoecker and W. Greiner, Phys. Rev. C **57**, 2576 (1998);

[48] G. A. Christos, Phys. Rev. D **35**, 330 (1987).

[49] P. Papazoglou, D. Zschiesche, S. Schramm, J. Schaffner-Bielich, H. Stoecker and W. Greiner, Phys. Rev. C **59**, 411 (1999).

[50] S. Schramm, Phys. Rev. C **66**, 064310 (2002).

[51] J. P. Blaizot, Phys. Rept. **64**, 171 (1980).

[52] P. Danielewicz, R. Lacey and W. G. Lynch, Science **298**, 1592 (2002).

[53] P. K. Sahu, W. Cassing, U. Mosel and A. Ohnishi, Nucl. Phys. A **672**, 376 (2000).

[54] M. Isse, A. Ohnishi, N. Otuka, P. K. Sahu and Y. Nara, Phys. Rev. C **72**, 064908 (2005).

[55] P. -G. Reinhard, M. Rufa, J. Maruhn, W. Greiner and J. Friedrich, Z. Phys. A **323**, 13 (1986); Suk-Joon Lee, J. Fink, A. B. Valantekin, M. R. Strayer, A. S. Umar, P. G. Reinhard, J. A. Maruhn and W. Greiner, Phys. Rev. Lett. **57**, 2916 (1986).

[56] G.A. Lalazissis, J. König and P. Ring, Phys. Rev. C **55**, 540 (1997).

[57] R. Brockmann and W. Weise, Phys. Lett. B **69**, 167 (1977).

[58] J. Boguta and S. Bohrmann, Phys. Lett. B **102**, 93 (1981).

[59] Y. Sugahara and H. Toki, Prog. Theor. Phys. **92**, 803 (1994); H. Shen, F. Yang and H. Toki, Prog. Theor. Phys. **115**, 325 (2006).

[60] J. Mareš and B. K. Jennings, Phys. Rev. C **49**, 2472 (1994).

[61] H. Lenske, Lect. Notes Phys. **641**, 147 (2004); C. M. Keil, F. Hofmann and H. Lenske, Phys. Rev. C **61**, 064309 (2000); C. Keil and H. Lenske, Phys. Rev. C **66**, 054307 (2002).

[62] H. Noumi *et al.*, Phys. Rev. Lett. **89**, 072301 (2002) [Erratum-ibid. **90**, 049902 (2003)]; P. K. Saha *et al.*, Phys. Rev. C **70**, 044613 (2004); T. Harada and Y. Hirabayashi, Nucl. Phys. A **759**, 143 (2005); T. Harada and Y. Hirabayashi, Nucl. Phys. A **767**, 206 (2006); M. Kohno, Y. Fujiwara, Y. Watanabe, K. Ogata and M. Kawai, Prog. Theor. Phys. **112**, 895 (2004); M. Kohno, Y. Fujiwara, Y. Watanabe, K. Ogata and M. Kawai, Phys. Rev. C **74**, 064613 (2006).

[63] S. Aoki *et al.*, Phys. Lett. B **355**, 45 (1995); T. Fukuda *et al.* [E224 Collaboration], Phys. Rev. C **58**, 1306 (1998); P. Khaustov *et al.* [AGS E885 Collaboration], Phys. Rev. C **61**, 054603 (2000); H. Maekawa, K. Tsubakihara and A. Ohnishi, Eur. Phys. J. A **33**, 269 (2007); H. Maekawa, K. Tsubakihara, H. Matsumiya and A. Ohnishi, arXiv:0704.3929 [nucl-th].

[64] S. Ajimura *et al.*, Phys. Rev. Lett. **86**, 4255 (2001).

[65] P. Finelli, N. Kaiser, D. Vretenar and W. Weise, Phys. Lett. B **658**, 90 (2007).

[66] I. H. Stairs, Science **304**, (2004) 547.

[67] R. Tamagaki, Prog. Theor. Phys. **119**, 965 (2008).

[68] Y. Yamamoto, S. Nishizaki and T. Takatsuka, Nucl. Phys. **A691**, 432 (2001).

[69] Y. Ogawa H. Toki, S. Tamenaga, H. Shen, A. Hosaka, S. Sugimoto and K. Ikeda, Prog. Theor. Phys. **111**, 75 (2004).

[70] C. J. Batty, E. Friedman and A. Gal, Phys. Lett. B **335**,

(1994) 273.
[71] J. Mareš, E. Friedman, A. Gal and B. K. Jennings, Nucl. Phys. A **594**, (1995) 311.
[72] M. Naruki *et al.*, Phys. Rev. Lett. **96**, 092301 (2006).
[73] K. Miura, T. Z. Nakano, A. Ohnishi, Prog. Theor. Phys. **122**, 1045 (2009): K. Miura, T. Z. Nakano, A. Ohnishi and N. Kawamoto, Phys. Rev. D **80**, 074034 (2009); T. Z. Nakano, K. Miura and A. Ohnishi, arXiv:0911.3453 [hep-lat].
[74] K. Tsubakihara, H. Maekawa and A. Ohnishi, Eur. Phys. J. A **33**, 295 (2007).
[75] C. J. Batty *et al.*, Phys. Lett. B **74** (1978) 27; R. J. Powers *et al.*, Phys. Rev. C **47**, 1263 (1993).
[76] N. Kaiser, S. Fritsch and W. Weise, Nucl. Phys. **A697**, 255 (2002). Y. Ogawa, H. Toki and S. Tamenaga, Phys. Rev. C **76**, 014305 (2007):
[77] T. Myo, K. Kato and K. Ikeda, Prog. Theor. Phys. **113**, 763 (2005); A. Isshiki, K. Naito and A. Ohnishi, Prog. Theor. Phys. **114**, 573 (2005).